International Journal of Energy Production and Management
https://www.acadlore.com/journals/IJEPM

# Numerical Analysis of Flame Propagation Parameters for Different Fuels

Hamza M. Mjbel[1], Ali M. Tukkee[1,2*], Haroun A. K. Shahad[3], Fatimah Malek Mohsen[4]

[1] Department of Petroleum Engineering, College of Engineering, University of Kerbala, 56001 Karbala, Iraq
[2] Air Conditioning and Refrigeration Techniques Engineering Department, University of Warith Al-Anbiyaa, 56001 Karbala, Iraq
[3] College of Engineering Technologies, University of Hilla, 51001 Hilla, Iraq
[4] Department of Mechanical Engineering, College of Engineering, University of Babylon, 51001 Hilla, Iraq

* Correspondence: Ali M. Tukkee (ali.muslim@uokerbala.edu.iq)

**Received:** 09-11-2025 **Revised:** 11-25-2025 **Accepted:** 12-15-2025

**Citation:** H. M. Mjbel, A. M. Tukkee, H. A. K. Shahad, and F. M. Mohsen, "Numerical analysis of flame propagation parameters for different fuels," *Int. J. Energy Prod. Manag.*, vol. 10, no. 4, pp. 686–700, 2025. https://doi.org/10.56578/ijepm100409.



**Abstract:** This study presents a comprehensive numerical analysis aimed at determining the enhanced combustion rate, burning velocity, and laminar flame speed of premixed LPG/air mixtures. Different values of equivalence ratios (ER) were considered between 0.6 and 1.4. The analyses were conducted at initial conditions of 1.0 atm and 300 K inside a horizontal cylindrical combustion chamber (CCC). Simulations were performed using ANSYS Fluent and Chemkin USC Mechanics 2.0 software, which effectively predicted flame characteristics. The results indicate that the stoichiometric mixture gives the highest extended laminar flame velocity of 288.88 cm/s, followed by the lean mixture, ER = 0.6, with 84.1 cm/s, and the rich mixture, ER = 1.4, with 118.66 cm/s. The observed combustion rates of the stoichiometric, lean, and rich mixtures were 14.9, 37, and 18.5 cm/s, respectively. Also, the laminar burning velocity for pure propane and pure butane at different ERs, of 0.6, 0.8, 1.0, 1.2, and 1.4, were 19.4, 36.9, 45, 42.1, and 25.1 for propane mixtures, and 14.8, 29, 36.5, 33.4, and 18.4 for butane mixtures, respectively. For the same aforementioned ER, the measured laminar flame velocities were 87.55, 200.9, 274.1, 238.9, and 116.67 cm/s, respectively, and the laminar combustion velocities were 15.2, 28.7, 35.5, 33, and 18.2 cm/s, respectively, with a 2.8% gain margin. Moreover, for naphtha fuel vapors, laminar combustion velocities of 32.16, 41.2, 49.45, 46, and 28.6 cm/s for ERs of 0.6, 0.8, 1, 1.2, and 1.4. The numerical results of the ILPG (Iraq liquefied petroleum gas) show that the maximum stretched laminar flame speed reached 288.88 cm/s at ER = 1.0, while with ER = 0.6, it is 84.1 cm/s, and with ER = 1.4, it is 118.66 cm/s. Compared to ILPG, propane, and butane, Naphtha burns faster.

**Keywords:** Combustion modeling; Flame propagation; Fuel-air mixture; Numerical simulation; Premixed fuel; Reaction kinematics

## 1 Introduction

The combustion process of fuel-air mixtures is a particularly important topic that was studied and analyzed experimentally and numerically in terms of flame speed and burning velocity by many researchers. Yang et al. [1] experimentally studied the propagation of lean $H_2$-CO-air flame premixed in a closed conduit under atmospheric conditions. Flame propagation was recorded using a fast camera. Tulip flame was observed in all cases; however, equivalency ratios and hydrogen blending ratios impacted tulip distortion. The flame front and speed were calculated via image processing. The results showed that flame-wall interaction and combustion instability also affect flame propagation dynamics; hence, the authors suggested that these elements should be considered when designing flame propagation models.

Park et al. [2] investigated flame characteristics of air-hydrogen, carbon monoxide, and saturated (C1-C4) hydrocarbon mixes both experimentally and numerically. They used a counter-flow arrangement to calculate flame velocities and ignition/extinction thresholds for premixed flames. USC Mech II's kinetic model was used in conjunction with the Chemkin software package to replicate the tests. Hydrocarbon additives were discovered to have unexpected effects on flame initiation, spread, and extinguishment when applied to hydrogen flames. It

was also shown that the reactivity of hydrogen flames is diminished when $C_3H_8$ or n-$C_4H_10$ substitutes for $CH_4$ during reignition or strong combustion. Fig et al. [3] explored flame propagation in the combustion of methane in horizontal cylindrical tubes both experimentally and computationally in relation to stoichiometry and tube diameter. Stoichiometric air/fuel circumstances saw an increase in burning velocities by a factor of 2–4 for ignitions at the closed end of the reactor, and this impact was also studied. Vertical tubes were utilized in the control area, whereas horizontal tubes with one end sealed off were employed in the experimentation part. Tubes with diameters from 5 centimeters to 71 centimeters were utilized. With ANSYS Fluent's two-dimensional numerical simulations, it was discovered that the maximum speed of a laminar flame's propagation rises with tube diameter. The results were in line with the observed patterns of flame velocities during experiments. Salem [4] used cylinder combustion to calculate hydrocarbon combustion using hydrogen gas and binary fuel. Simple mechanisms were used to simulate a 2D cylindrical tube 40 cm long and 2 cm in diameter. Several hydrocarbon/air and synthetic gas simulations were performed using a fine quadrilateral grid within 7 cm of the tube's length and the surrounding walls to see the flame's features in action.

Ströhle and Myhrvold [5] used the Chemkin program to determine that the intensity of the laminar flame is a significant factor in determining the rate at which the flames of the premixed combustion spread. He et al. [6] used combined experimental observations and kinetic models to investigate the effects of $H_2$ concentration on the laminar flame velocities of typical syngas. Kinetic simulations were performed in CHEMKIN using two mechanisms, GRI-Mech 3.0 and USC-Mech II, while the flame area was measured using the Bunsen technique from OH planar laser-induced fluorescence (OH-PLIF) pictures. Both techniques produced predictions that were generally consistent with data, particularly under fuel-lean situations. At U = 0.8 and 0.9, USC-Mech II simulations showed greater agreement with experimental results (discrepancy 5%). Shakir [7] measured laminar flame speed in a centrally fired constant-volume cylindrical chamber heated to 308 K and compressed to 0.1 to 0.3 MPa using a premixed LPG/$H_2$/air mixture. Hydrogen mixing ratios by mass from 0 to 80% with different equivalence ratios (ER) were studied. Combustion characteristics included laminar flame speed, chamber pressure, velocity, and expansion.

Han et al. [8] examined the influence of Soret diffusion (SD) on turbulent non-premixed $H_2$ combustion by comparing two three-dimensional direct numerical simulations of time-varying turbulent jet flames. A Mixture-averaged Diffusion (MD) model replicated the multicomponent transport and SD effects (MD combined with a Soret term). Their study focused on SD's influence on flame tangential diffusion and differential diffusion. The results showed that SD significantly affected H and OH mass fractions. SD has a small influence on temperature, heat release rate, and $H_2$ mass fraction because a larger SD flow of H radical is strongly linked to fundamental chemical reactions. Li et al. [9] studied $H_2$/air mixture focusing on mixing performance, flame stability limit, and combustion efficiency. They were evaluated numerically in a 2D planar micro-combustor with a separating plate at three different inlet velocities and channel heights (0.6 mm, 1.0 mm, and 1.4 mm). Based on the findings, it was determined that reducing the inflow velocity and channel height would increase the mixing efficiency. It was also shown that a 0.6 mm flame blow-off limit is the maximum possible for a micro-combustor. The flame gets skewed when the input speed is high, and the flame's orientation shifts constantly. Results also showed that at constant intake velocities, reducing the combustor's height improved its combustion efficiency. Baudoin et al.[10] evaluated the stabilization and local extinction structures of partly premixed $CH_4$/air flames using simultaneous OH-PLIF/PIV and large eddy simulations using a two-scalar flamelet model. The mixing and combustion chamber has two concentric tubes, and the mixing length controls partial premixing. Flame stability regimes were found for various partial premixing and Reynolds numbers. Reduced partial premixing of air to the fuel stream stabilized flames at low Reynolds numbers. The flame was found to be most stable at a certain partial premixing threshold at high Reynolds numbers. Experimental results showed considerable local extinction gaps for stable flames beyond the blowout phase. Faghih and Chen [11] used CVM and CPM to study flame growth. Comparing these two approaches' outcomes, they found large differences in laminar flame speed measured by CVM and focused on data processing errors. They concluded that this method could measure laminar flame speed at high pressures and temperatures close to engine-relevant conditions.

Liu et al. [12] investigated the effects of oxygen enrichment on the laminar flame speed of methane and ammonia mixtures at atmospheric pressure and a starting temperature of 300 K, with varying mixture composition. Laminar flame speed was shown to be negatively correlated with $CO_2$ concentration and positively correlated with $O_2$ concentration. The ammonia impact was likewise shown to be proportional to the mixture's equivalency ratio. Fig et al. [3] conducted an experimental and computational study of $CH_4$ combustion and flame propagation in a horizontal cylindrical chamber. They analyzed stoichiometry, cylinder size, and ignition placement. They determined that the maximum speed at which a laminar flame could flow in a tube depended directly on its diameter. The stoichiometric uniform burning velocity was shown to have a linear and functional relationship with the tube diameter. Movaghar et al. [13] used numerical simulations to better understand flame front propagation with a centrally ignited expanding flame in a closed-volume burner (CVC). The results indicated that the flame radius significantly affects the laminar flame speed, stressing the necessity for correct modeling of the flame radius by considering different parameters.

Hu and Wei [14] investigated (both mathematically and experimentally) the laminar flame speed of propane

($C_3H_8$) in an $O_2/CO_2$ environment. It was discovered that the speed of a laminar flame gradually increased with increasing $O_2$ concentration. The findings demonstrated that the physical properties of $CO_2$ have a more substantial impact than their chemical counterparts. Brune [15] compared the average speeds at which methane flames burned in a number of different-sized reaction containers. The experiments were conducted to verify the computational fluid dynamics (CFD) model and to set a standard against which the performance of the vessels may be measured after obstructions have been introduced. Wang et al. [16] used the $k-\varepsilon$ turbulence model, Zimont premixed combustion model, and SIMPLE algorithm to analyses the propagation velocity and pressure of the premixed methane-air flame in a half-open square tube with three solid obstacles. Simulations indicated that the triangular prism obstacle at a 40% blockage ratio accelerated flame and airflow, and its propagation velocity and deflagration pressure were somewhat higher than cuboid and cylinder obstacles.

Jager et al. [17] used ANSYS Fluent software to conduct a 2D simulation for the evaluation of flame stability in premixed hydrogen-air combustion. The study proved that the model can be used for designing efficient surface-stabilized burners. Cisneros and Rojas [18] used numerical methods to analyze 12 combustion products, flame temperature, and laminar burning velocity of LPG. The authors adopted MATLAB and ANSYS CHEMKIN software to accomplish their study. The results obtained from the two software programs agreed with each other and with experimental results, which proved the feasibility of the analysis. Mjbel [19] performed an experimental study to measure the laminar flame speed for premixed Iraqi LPG-air mixtures at different ER ranging from 0.6 to 1.4 in a horizontal cylindrical combustion chamber (CCC). Their results showed that the flame speed increases with the equivalence ratio up until stoichiometric, then the flame speed starts decreasing as the mixture becomes richer.

In this study, Ansys Fluent and Chemkin software are used to analyze the flame propagation parameters for different fuels and under different values of ER. The combustion model is simulated as a horizontal cylinder, which represents the combustion chamber. The fuels considered are pure propane, pure butane, ILPG, and Naphtha.

## 2 Numerical Methodology

### 2.1 ANSYS Fluent Program

Versteeg [20] indicated that the use of CFD to anticipate internal and exterior flow characteristics has increased dramatically in recent years. Therefore, ANSYS 17 and CHEMKIN CFD software were used in this study. Three of the many procedures found in this software package served as the basis for this investigation. The first two were employed for geometric modeling, while the third was put to use for simulating fluid dynamics, heat transport, chemical reactions, and combustion.

#### 2.1.1 Governing equations

The solution of the present problem is governed by three governing equations, which are: Mass Conservation Equation, Momentum Conservation Equation, and Energy Conservation Equation. The software solves these equations iteratively.

**Mass Conservation Equation**

We may write the continuity equation as:

$$\frac{\partial \rho}{\partial t}+\frac{\partial(\rho u)}{\partial x}+\frac{\partial(\rho v)}{\partial y}+\frac{\partial(\rho w)}{\partial z}=0 \tag{1}$$

where,

$\rho$ = density of fluid,

$t$ = time,

$u, v, w$ = components of velocity in $x, y$ and $z$, respectively.

The dynamics of compressible fluids in three dimensions are described by Eq. (1). The first term in equation (1) represents the rate of change of density (mass per unit volume); the second term, known as the convective term, depicts the net flow of mass away from the element along its borders [21, 22].

**Momentum Conservation Equation**

The three-dimensional momentum equations are,

• The $x$-axis equation:

$$\rho \frac{Du}{Dt}=\frac{\partial\left(-P+\tau_{xx}\right)}{\partial x}+\frac{\partial \tau_{yx}}{\partial y}+\frac{\partial \tau_{zx}}{\partial z}+S_{Mx} \tag{2}$$

• The $y$-axis equation:

$$\rho \frac{Dv}{Dt}=\frac{\partial\left(-P+\tau_{xy}\right)}{\partial x}+\frac{\partial \tau_{yy}}{\partial y}+\frac{\partial \tau_{zy}}{\partial z}+S_{My} \tag{3}$$

• The $z$-axis equation:

$$\rho\frac{Dw}{Dt}=\frac{\partial\left(-P+\tau_{xz}\right)}{\partial x}+\frac{\partial\tau_{yz}}{\partial y}+\frac{\partial\tau_{zz}}{\partial z}+S_{Mz} \tag{4}$$

where,

$P$ = static pressure.

$\tau_{ij}$ = The i.normal to the surface, j.normal component of the viscous stress operates.

$S_{Mi}$ = gravitational body force in i-direction.

Since tensile stress is typically considered the positive normal stress, the minus sign associated with pressure may be explained by the fact that, by definition, compressive normal stress is greater than the tensile normal stress. Explicit consideration is given to the role that surface tensions play. Forces exerted by the body are the sole sources of energy used in Eqs. (2-4), denoted by the source terms $S_{Mx}$, $S_{My}$ and $S_{Mz}$. For instance, if we were to represent the force exerted on our bodies by gravity, we could write $S_{Mx}=0$, $S_{My}=0$, $S_{Mz}=g$.

Deformation increases the viscous strains in Newtonian fluids. Both the dynamic viscosity, which relates stresses to linear deformations, and the viscosity, which relates stresses to volumetric deformations, are proportional constants needed by Newton's law of viscosity to describe compressible flow in three dimensions. Components of viscous stress are connected.

**Energy Conservation Equation**

The fluid particles change in energy per unit volume is:

$$\begin{aligned}\rho\frac{\partial E}{\partial t}=-(P\vec{V})+\Bigg[&\frac{\partial\left(u\tau_{xy}\right)}{\partial x}+\frac{\partial\left(u\tau_{yy}\right)}{\partial y}+\frac{\partial\left(u\tau_{zy}\right)}{\partial z}\\&+\frac{\partial\left(v\tau_{xy}\right)}{\partial x}+\frac{\partial\left(v\tau_{yy}\right)}{\partial y}+\frac{\partial\left(v\tau_{zy}\right)}{\partial z}\\&+\frac{\partial\left(w\tau_{xy}\right)}{\partial x}+\frac{\partial\left(w\tau_{yy}\right)}{\partial y}+\frac{\partial\left(w\tau_{zy}\right)}{\partial z}\Bigg]\end{aligned} \tag{5}$$

If any source of energy exists with $S_E$ energy per unit volume per unit time, the energy equation becomes:

$$\begin{aligned}\rho\frac{\partial E}{\partial t}=-(P\vec{V})+\Bigg[&\frac{\partial\left(u\tau_{xy}\right)}{\partial x}+\frac{\partial\left(u\tau_{yy}\right)}{\partial y}+\frac{\partial\left(u\tau_{zy}\right)}{\partial z}\\&+\frac{\partial\left(v\tau_{xy}\right)}{\partial x}+\frac{\partial\left(v\tau_{yy}\right)}{\partial y}+\frac{\partial\left(v\tau_{zy}\right)}{\partial z}\\&+\frac{\partial\left(w\tau_{xy}\right)}{\partial x}+\frac{\partial\left(w\tau_{yy}\right)}{\partial y}+\frac{\partial\left(w\tau_{zy}\right)}{\partial z}\Bigg]\\&+(K\nabla T)+S_E\end{aligned} \tag{6}$$

**General Transport Equation**

There are numerous similarities across fluid flow equations, and they may all be stated conservatively:

$$\frac{\partial(\rho\Phi)}{\partial t}+(\rho\Phi\vec{V})=(\Gamma\nabla\Phi)+S_\Phi \tag{7}$$

The property transfer equation, denoted by (7), emphasizes several types of transport, including the convective and diffusive processes on the left and the rate of change term and the diffusion coefficient on the right.

The standard $k$–$\varepsilon$ turbulence model was adopted in the solution. The model's goal is to provide a mathematical description of turbulence and viscosity in terms of the corresponding production and destruction equations. The empirical method relies on the use of experimental data to build relationships. The turbulent viscosity is defined for $k$–$\varepsilon$ models as:

$$\mu_t=\bar{\rho}C\mu\frac{k^2}{\varepsilon} \tag{8}$$

Two equilibrium equations, one for each $k$ and $\varepsilon$, are solved to characterize them.

$$\frac{\partial}{\partial t}(\bar{\rho}K)+\frac{\partial}{\partial x_i}\left(\bar{\rho}\widetilde{u}_\imath K\right)=\frac{\partial}{\partial x_i}\left[\left(\mu+\left(\mu t\frac{\mu_t}{\sigma_k}\sigma k\right)\frac{\partial k}{\partial x_i}\right]+P_K-\bar{\rho}_\varepsilon\right. \tag{9}$$

$$\begin{aligned}\frac{\partial}{\partial t}(\bar{\rho}\varepsilon)+\frac{\partial}{\partial x_i}\left(\bar{\rho}\widetilde{u}_\imath\varepsilon\right)=&\frac{\partial}{\partial x_i}\left[\left(\mu+\mu t\frac{\mu_t}{\sigma_k}\sigma\varepsilon\right)\frac{\partial\varepsilon}{\partial x_i}\right]+C_{\varepsilon1}\varepsilon\frac{\varepsilon}{\mathrm{k}}P_k\\&-C_\varepsilon2\bar{\rho}\frac{\varepsilon^2}{k}\end{aligned} \tag{10}$$

The source term $P_K$ is given by:

$$P_K = -\bar{\rho}\widetilde{u''_i u''}\frac{\partial \tilde{u}''_i}{\partial x_j} \tag{11}$$

Table 1 gives the predefined values for the constants of the standard $k$–$\varepsilon$ turbulence model.

**Table 1.** Values of the constant used in the standard $k$–$\varepsilon$ turbulence model

| Constant Symbol | Value |
|---|---|
| $C_\mu$ | 0.09 |
| $C_{\epsilon 1}$ | 1.44 |
| $C_{\epsilon 2}$ | 1.92 |
| $\sigma_k$ | 1.0 |
| $\sigma_\epsilon$ | 1.0 |

2.1.2 The combustor model and mesh construction

CFD simulation begins with fluid flow analysis model preparation. Geometric substitutes like tetrahedral cells divide the flow domain. Then, each subdomain's governing equations are solved. A high-quality mesh produces a higher accuracy for the numerical solution, hence it is desired in complicated flow fields. High-quality networks enhance convergence and CFD solution correctness. Here, the combustion model is simulated as a horizontal cylinder (Combustion chamber) with six openings to introduce a premixed LPG/air mixture, as shown in Figure 1.

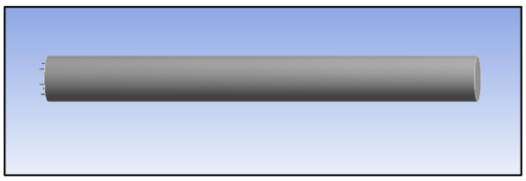

**Figure 1.** The combustor geometry

Three levels of unstructured tetrahedral mesh are generated with grid sizes of 2, 5, and 8 mm, where the mesh form of the grid size of 5 mm is shown in Figure 2a. For each scenario, the maximum inflation layer is 20 layers and is shown in Figure 2b. The list of meshes is shown in Table 2. The number of iterations required to achieve convergence ranged from 1,500 to 2,000 iterations.

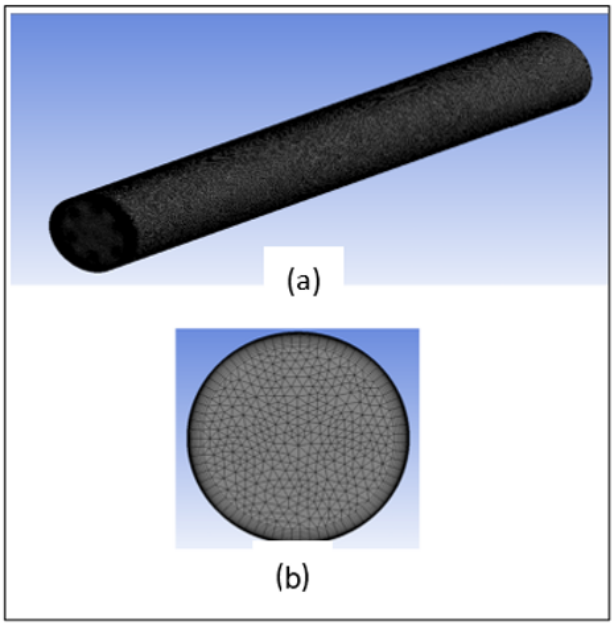


**Figure 2.** Combustion Chamber Mesh Generation: (a) the entire combustion chamber; (b) cross-sectional area of the combustion chamber

**Table 2.** Meshing details

| No. of Mesh | Mesh Size | Number of Nodes | Number of Elements | Run Time (hr.) |
|---|---|---|---|---|
| 1 | 2 mm | 3,830,582 | 22,195,923 | 72 |
| 2 | 5 mm | 1,124,248 | 3,522,630 | 30 |
| 3 | 8 mm | 446,830 | 1,216,049 | 5 |

#### 2.1.3 Boundary conditions in combustion simulations

After the mesh dependency is evaluated, the combustion model is used to simulate the combustion of ILPG under premixed conditions. All CFD analyzes are performed using an entry velocity of 0.022 m/s. An adiabatic premixed combustion model is assumed in this work. Premixing is modeled using the Finite-Rate/Eddy-Dissipation Model. A simplified combustion model consists of 5 chemical forward reactions and 13 species for each ER. The forward reactions considered in the present study are:

$0.558\mathrm{C_3H_8} + 0.442\mathrm{C_4H_{10}} + 4.37\mathrm{O_2} \rightarrow 3.442\mathrm{CO} + 4.442\mathrm{H_2O}$

$K_f = 6.364 \times 10^{23} \exp[-30194.9/\mathrm{T}]\,[C_3\mathrm{H_8}]^{0.1}\,[\mathrm{C_4H_{10}}]^{0.15}\,[\mathrm{O_2}]^{1.63}$

$3.442\mathrm{CO} + 1.721\mathrm{O_2} \rightarrow 3.442\mathrm{CO_2}$

$K_f = 10^{19.85} \exp[-20142/\mathrm{T}][\mathrm{CO}]^1\,[\mathrm{H_2O}]^{0.5}\,[\mathrm{O_2}]^{0.25}$

$\mathrm{O_2} + 2\,\mathrm{N_2} \rightarrow 2\,\mathrm{N} + 2\mathrm{NO}$

$K_f = 1.5587 \times 10^{14} \exp[-67627/\mathrm{T}][\mathrm{CO}]^1\,[\mathrm{H_2O}]^1\,[\mathrm{O_2}]^2$

$2\mathrm{O_2} + \mathrm{N_2} \rightarrow 2\mathrm{O} + 2\mathrm{NO}$

$K_f = 2.6484 \times 10^{19} \exp[-59418/\mathrm{T}]\,[\mathrm{N_2}]^1\,[\mathrm{O_2}]^2$

$\mathrm{N_2} + 2\mathrm{OH} \rightarrow 2\mathrm{H} + 2\mathrm{NO}$

$K_f = 2.123 \times 10^{14} \exp[-57020/\mathrm{T}][\mathrm{OH}]^2[N]^2$

where, the forward reaction rate, $K_t$, is expressed in $\mathrm{kmole/m^3 \cdot\ s}$, the temperature, T, is in Kelvin (K), and $\phi = 1$ is the ER.

The laminar flame speed can be predicted by calculating the rate of reaction from the ANSYS Fluent program and thermal diffusivity, using the engineering equations solver (EES) program, and substituting in Eq. (12):

$$S_L = \sqrt{2 \times \alpha \times (u_r + 1) \times \frac{R_r}{\rho_u}} \tag{12}$$

where, $\alpha$ is the thermal diffusivity ($\mathrm{m^2/s}$), $u_x$ is the air to fuel mass ratio, $e_u$ is the unburnt mixture density ($\mathrm{kmole/m^3}$), and $R_r$ is the rate of reaction ($\mathrm{kmole/m^2.s}$)

The reaction rate is explained in Eq. (13).

$$\text{Rate of reaction } = K[A]^n[B]^m \tag{13}$$

$$K = A_p T^{\beta} \left[\frac{-E}{RT}\right] \tag{14}$$

where, $K$ is the reaction rate coefficient, $A_p$ is the preexponential factor, $E$ is the activation energy, $R$ is the universal gas constant, $\beta$ is the temperature exponent, $T$ is the temperature, $[A][B]$ is the concentration of the reactants, and $n, m$ are reaction rank.

### 2.2 Coding in CHEMKIN Software

One of the most widely used programs for modeling chemical processes and analyzing kinetics is CHEMKIN-PRO. In this study, we model the flame speed of a premixed ILPG/air flame in a horizontal CCC using the CHEMKIN-PRO program. Researchers analyze how changes in the equivalency ratio and chemical composition of ILPG affect the rate of flame expansion. Combustion chamber entry conditions for the ILPG/air mixture are 1 bar and 300 K. The equivalency ratio examined is between 0.6 and 1.4. There are 111 species and 784 reactions in the CHEMKIN software's reaction mechanism [23, 24]. Some of these reactions are shown below as examples:

$\mathrm{n - C_3H_2} \rightarrow \mathrm{C_2H_4} + \mathrm{CH_3}$ (R1)

$\mathrm{C_2H_4} + \mathrm{H} + \mathrm{M} \rightarrow \mathrm{C_2H_2} + \mathrm{M}$ (R2)

$\mathrm{C_2H_2} + \mathrm{H} \rightarrow \mathrm{CH_3} + \mathrm{CH_3}$ (R3)

$\mathrm{p - C_4H_2} \rightarrow \mathrm{C_2H_4} + \mathrm{C_2H_5}$ (R4)

$i - C_3H_2 + O \rightarrow CH_3CHO + CH_2$ (R5)
$CH_3CHO + X \rightarrow CH_3CO + XH$ (R6)
$CH_3CO \rightarrow CH_3 + CO$ (R7)
where, X stands for H, O, or $OH\_CH_3$

The velocity of the reactants entering the combustion chamber is determined as:

$$\dot{Q} = A \cdot V \tag{15}$$

where, $\dot{Q}$ is the mixture volume flow rate $\left(\mathrm{m}^3/\mathrm{s}\right)$, $V$ is the inlet velocity $(\mathrm{m/s})$, $A$ is the total mixture inlet ports area $(\mathrm{m}^2)$, and n is the number of inlet ports.

The following assumptions are made for running the ANSYS Fluent and Chemkin programs:

1- Using a Premixed ILPG/air mixture

2- The atmospheric air consists of $O_2$ and $N_2$ with a ratio of (21:79) by volume.

3- Uniform overall equivalent ratio.

4- Neglecting the dissociation process of the product.

5- The flow is one-dimensional at using ANSYS CHEMKIN, and three-dimensional at using ANSYS Fluent.

6- The temperature and pressure of the mixture are initially constant and uniform; $(T_{\mathrm{u}} = 298\ \mathrm{K})$ and $(\mathrm{P}_i = 1\mathrm{bar})$ for all experimental tests.

7- Inlet mixture velocity is constant for each test.

8- The flow is laminar.

Two important parameters were considered in the current study, the laminar flame speed and the laminar burning velocity. The laminar flame speed is the rate of expansion of the flame front in a combustion reaction. The laminar burning velocity, on the other hand, is a fundamental measure describing how a plane flame propagates through a stationary, unburned mixture in front of it at a given pressure and temperature.

## 3 Results and Discussion

The results of the present work are the response rate, laminar burning velocity, laminar flame speed, and adiabatic flame temperature by KEMKIN and ANSYS FLUENT software for premixed mixtures of different fuels with air, including ILPG, propane, butane, and Naphtha. Mixtures of different equivalent ratios, ranging from (0.6–1.4), are investigated. In this study, the ILPG is assumed to consist of propane and butane only, and other species are neglected because their mole fractions are extremely low.

### 3.1 Analysis of ANSYS/CHEMKIN Results

A comparison of the variation of adiabatic flame temperatures with ER for propane, LPG, butane, and Naphtha is depicted in Figure 3. It is demonstrated that the adiabatic flame temperature of propane is the highest, followed by ILPG and then butane. This is because propane has the greatest LCV of any fuel currently in use. The highest temperature is for the stoichiometric combination for all the fuels because all of the fuel is burnt completely during the combustion process, and the amount of air is just that required for combustion.

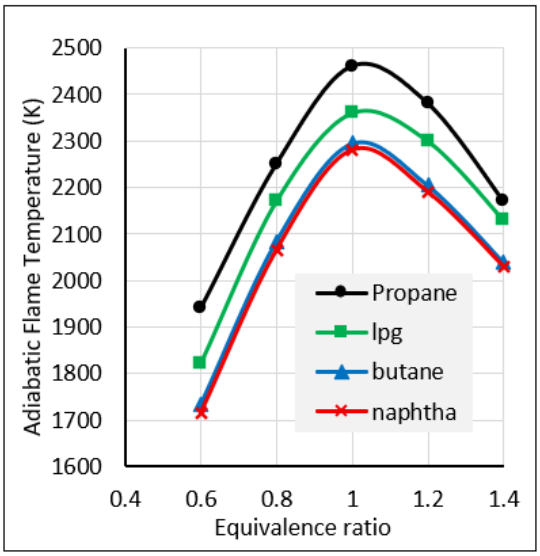


**Figure 3.** Adiabatic flame temperature versus equivalence ratio (ER) for various fuels

Figure 4 depicts how the laminar flame speed for the ILPG-air combination varies with the ER. It can be shown that the speed of a laminar flame rises on the lean side, peaks at ER = 1, then falls off as the mixture grows richer. All other fuels show the same trends, but with different values of flame speed.

The inverse density ratio is used to determine the laminar burning velocity for all fuels. The results are shown in Figure 5. The figure demonstrates how ER affects laminar burning velocity. The chart indicates that all fuels' burning velocity is highest for the stoichiometric mixture and falls for lean and rich mixtures. For all ER values, pure propane burns fastest, followed by ILPG and then pure butane, followed by Naphtha. This is attributed to the effect of burning temperature since the burning velocity is strongly temperature dependent, which means that the mixture that has a higher burning temperature burns faster. The burning velocity obtained by the ANSYS CHEMKIN program in this work is compared with the results of Akram et al. [25], as shown in Figure 6. The comparison shows an acceptable agreement. The slight differences are due to the difference in the chemical composition of LPG in both research and the difference in the mixture supply velocity to the combustion chamber. In the ILPG, the propane mole fraction is 0.55, and the entry velocity is 0.022 m/s, while in the other work, the propane mole fraction is 0.40 and the entry velocity is 0.5 m/s.

Figure 7 shows a comparison between the results of the current study obtained from CHEMKIN and the experimental results presented by Mjbel [19]. The comparison is made in terms of the flame velocity, and it can be seen that the results are remarkably close, with an acceptable margin of difference that can be attributed to inaccuracies in laboratory measurements.

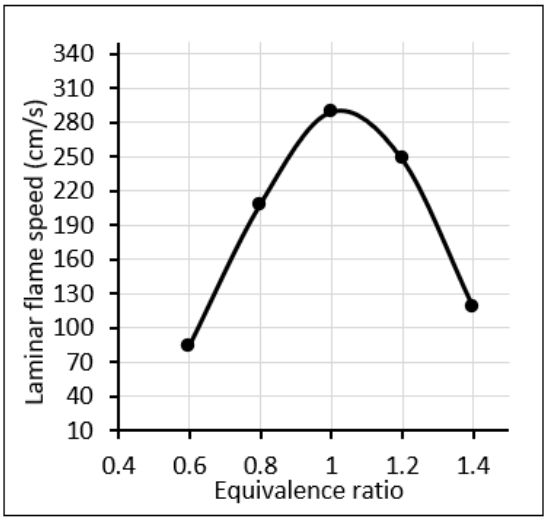


**Figure 4.** Laminar flame speed of ILPG-Air with ER

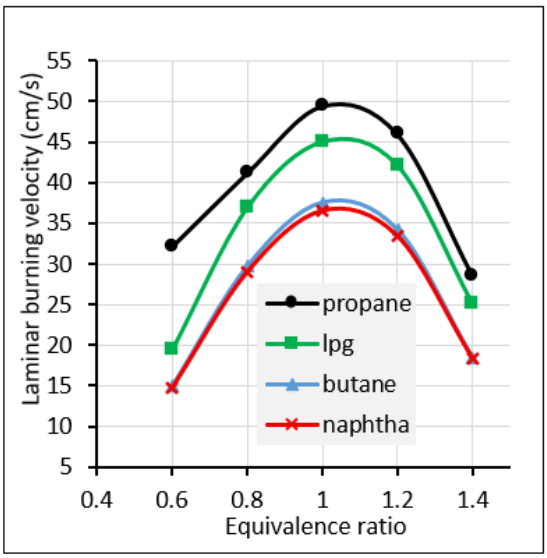


**Figure 5.** Laminar burning velocity versus ER for different fuels

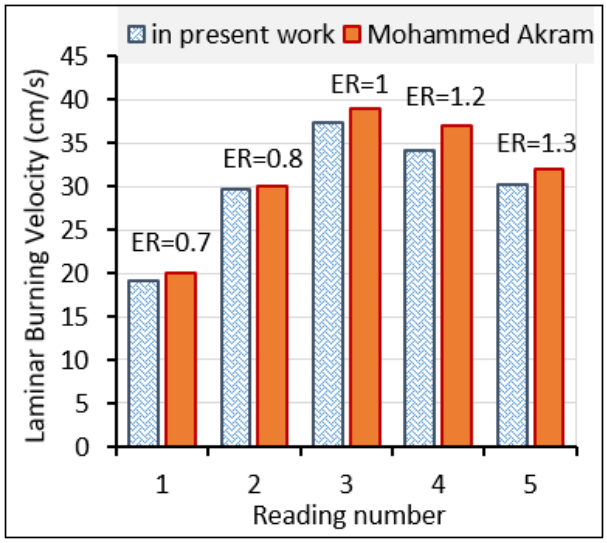


**Figure 6.** Laminar burning velocity versus ER for different fuels

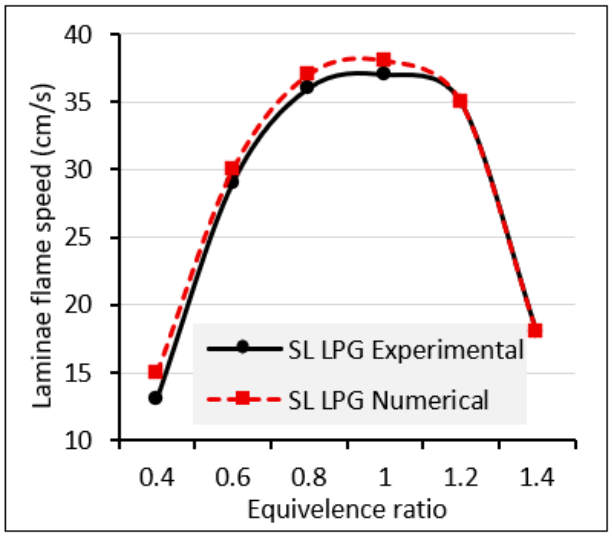


**Figure 7.** A Comparison between the results obtained from CHEMKIN and experimental data presented by Mjbel [19]

### 3.2 Analysis of ANSYS Fluent Results

Figure 8 shows the effect of ER on the adiabatic flame temperature for ILPG. From the figure, we can see that the maximum adiabatic flame temperature results from the stoichiometric mixture. The lower temperature for the lean mixture is due to less heat release per unit mass of mixture, and the lower temperature for the rich mixture is due to incomplete combustion of fuel due to insufficient oxygen. This is the same trend as obtained by ANSYS CHEMKIN.

Figure 9 shows the ILPG-AIR mixture laminar flame speed change with ER. According to the figure, the laminar flame speed was highest for the stoichiometric combination and decreased for lean and rich mixtures.

Figure 10 shows the variation of inverse density ratio, $\rho_b/\rho_u$, at various ER for ILPG fuel. The inverse density ratio is calculated on the basis of the adiabatic flame temperature obtained from the ANSYS FLUENT program and the unburnt mixture temperature. It is shown that the inverse density ratio is minimum for the stoichiometric mixture due to its high combustion temperature, while the inverse density ratio is high for lean and rich mixtures due to their lower combustion temperature.

Figure 11 displays the effect of ER on laminar burning velocity for the ILPG/air mixture. The laminar burning velocity is obtained on the basis of the inverse density ratio. Obviously, the stoichiometric combination burns fastest, while lean and rich mixes burn slower. This is because the stoichiometric combination has the maximum flame temperature (refer to Figure 8), and burning velocity is strongly temperature dependent.

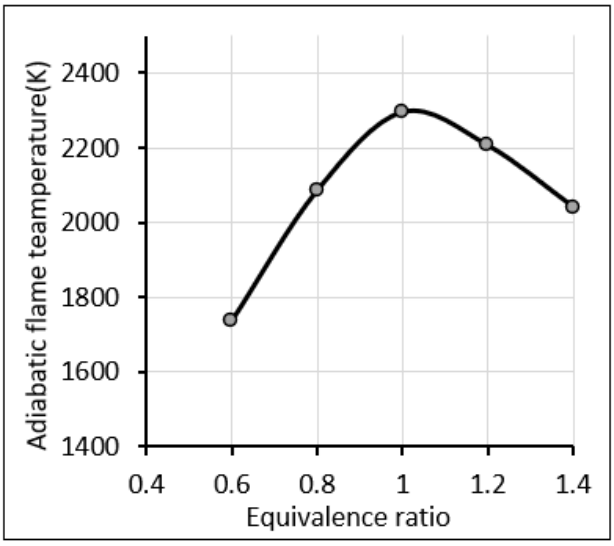


**Figure 8.** Effect of ER on adiabatic flame temperature

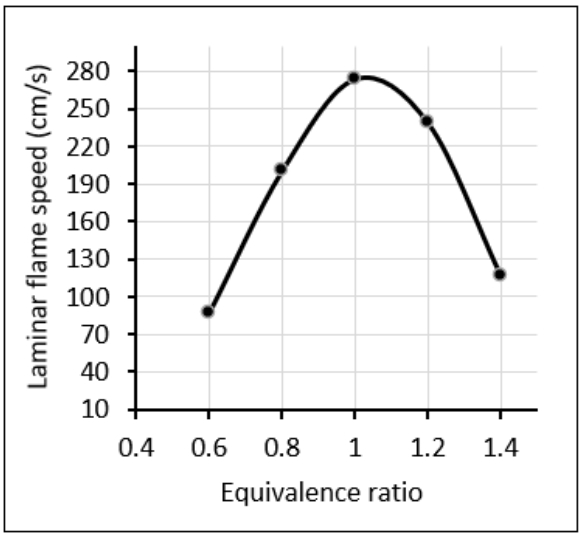


**Figure 9.** Laminar flame speed with ER

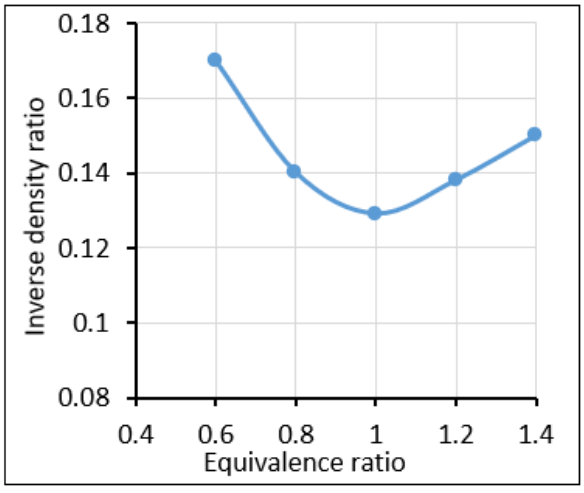


**Figure 10.** Inverse density ratio of ILPG-Air mixture combustion

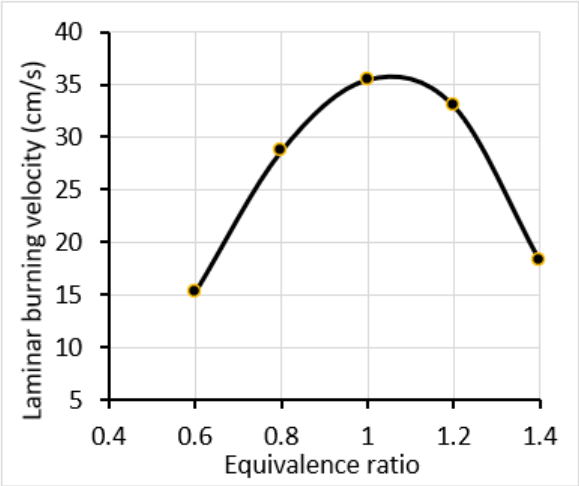


**Figure 11.** Inverse density ratio of ILPG-Air mixture combustion

Figure 12 presents the variation of burning velocity and reaction rate with ER. It is noticed that both the burning velocity and the reaction rate are ER-dependent. The figure shows that the reaction rate and the burning velocity reach their maximum value with the stoichiometric mixture, while they decrease for the lean and rich mixtures. This is due to the high flame temperature of the stoichiometric mixture.

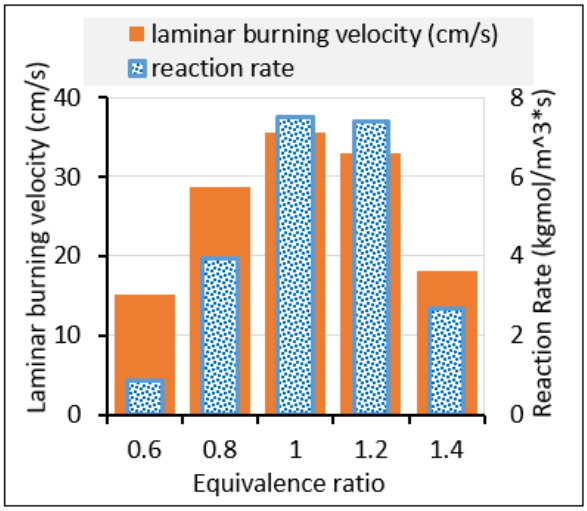


**Figure 12.** Laminar burning velocity with reaction rate versus ER

Figure 13 shows the temperature contours along the combustion chamber until exit. It is noticed that the temperature at the fuel inlet, at 5 cm along the CCC, is equal to room temperature (300 K). After 5 cm, where the ignition source is located, and further down the CCC, the temperature increases rapidly due to the combustion. The maximum temperature of (2260 K) is attained at about 45 cm along the CCC and then decreases further down until exit, since most of the fuel is burnt and due to air dilution.

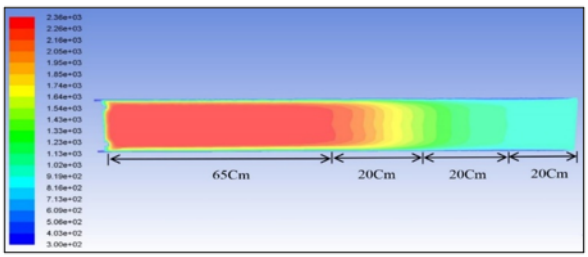


**Figure 13.** Temperature contours

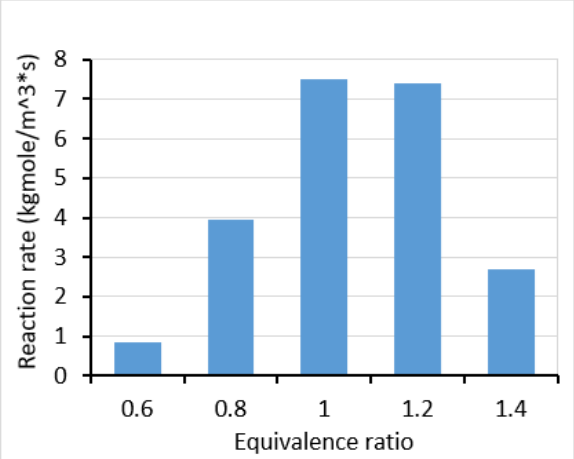


**Figure 14.** Variation of reaction rate with ER

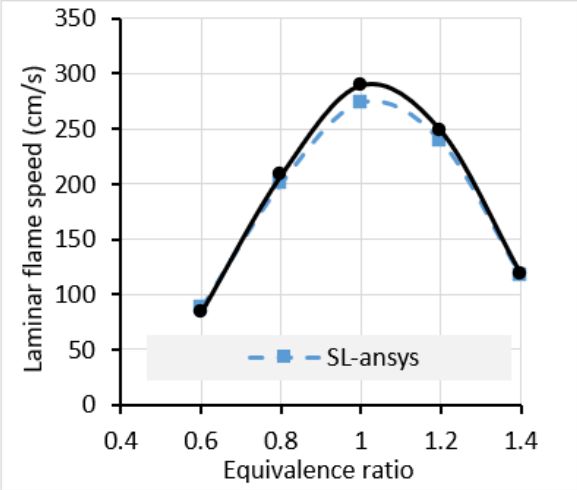


**Figure 15.** Comparison between the numerical laminar flame speed of both programs

Figure 14 presents the variation of the reaction rate with ER. It is indicated that the variation of reaction is the same as that of burning velocity since both are temperature dependent. The stoichiometric mixture has the highest rate and decreases for rich and lean mixtures.

Figure 15 presents a comparison between the numerical laminar flame speed obtained from both programs for ILPG fuel. It is noticed that the results are remarkably close, with an exceedingly small error of about 5%.

## 4 Conclusions

The current study provides a validated computational framework combining ANSYS Fluent and CHEMKIN for analyzing flame propagation across several hydrocarbon fuels and demonstrates how changes in ER govern burning behavior. These findings may support future design work in premixed combustion systems. The most significant conclusions drawn from the results of this investigation are:

• The maximum laminar burning velocity and that of the stretched laminar flame speed for all fuels occur at the stoichiometric mixture for both models. The maximum burning velocities are 45 m/s, 37.4 m/s, and 36.5 m/s for propane, ILPG, and butane, respectively.

• The maximum laminar burning velocity for ILPG is higher than that of naphtha vapor at a stoichiometric mixture. The maximum stretched laminar flame speed for ILPG at a stoichiometric mixture is equal to 274.06 cm/s.

• The ER has a very noticeable effect on the laminar burning velocity and stretched laminar flame speed.

• The maximum rate of reaction occurs for stoichiometric mixtures, and the stretched laminar flame speed increases with the increase in reaction rate.

• The initial stretched laminar flame speed is high, close to the ignition source and decreases slightly along the CCC until reaching a constant value at about 40 cm down the CCC.

• The maximum temperature occurs close to the ignition source and remains constant until about 40 cm down the CCC, and then it decreases due to combustion termination and air pollution.

## Data Availability

The data used to support the findings of this study are available from the corresponding author upon request.

## Conflicts of Interest

The authors declare that they have no conflicts of interest.

## References


[1] X. Yang, M. Yu, K. Zheng, P. Luan, and S. Han, "On the propagation dynamics of lean H2/CO/air premixed flame," *Int. J. Hydrogen Energy*, vol. 45, no. 11, pp. 7210–7222, 2020. https://doi.org/10.1016/j.ijhydene.2019.12.116

[2] O. Park, P. S. Veloo, N. Liu, and F. N. Egolfopoulos, "Combustion characteristics of alternative gaseous fuels," *Proc. Combust. Inst.*, vol. 33, no. 3, pp. 887–897, 2011. https://doi.org/10.1016/j.proci.2010.06.116

[3] M. K. Fig, G. E. B. Jr., J. F. Brune, and J. W. Grubb, "Experimental and numerical investigation of methane ignition and flame propagation in cylindrical tubes ranging from 5 to 71 cm – Part I: Effects of scaling from laboratory to large-scale field studies," *J. Loss Prev. Process Ind.*, vol. 41, pp. 241–251, 2016. https://doi.org/10.1016/j.jlp.2016.03.018

[4] E. K. Salem, "Numerical simulations of premixed flames of multi component fuels/air mixtures and their applications," Ph.D. Dissertation, University of Kentucky, 2018.

[5] J. Ströhle and T. Myhrvold, "An evaluation of detailed reaction mechanisms for hydrogen combustion under gas turbine conditions," *Int. J. Hydrogen Energy*, vol. 32, no. 1, pp. 125–135, 2007. https://doi.org/10.1016/j.ijhydene.2006.04.005

[6] Y. He, Z. Wang, L. Yang, R. Whiddon, Z. Li, J. Zhou, and K. Cen, "Investigation of laminar flame speeds of typical syngas using laser based bunsen method and kinetic simulation," *Fuel*, vol. 95, no. 3, pp. 206–213, 2012. https://doi.org/10.1016/j.fuel.2011.09.056

[7] A. Shakir, "Experimental study of the effect of hydrogen blending on burning velocity of different fuels," Master's thesis, University of Babylon, 2016.

[8] W. Han, A. Scholtissek, F. Dietzsch, and C. Hasse, "Effects of Soret diffusion on turbulent non-premixed H2 jet flames," *Combust. Flame*, vol. 213, pp. 39–51, 2020. https://doi.org/10.1016/j.combustflame.2019.11.029

[9] L. Li, Z. Yuan, Y. Xiang, and A. Fan, "Numerical investigation on mixing performance and diffusion combustion characteristics of H2 and air in planar micro-combustor," *Int. J. Hydrogen Energy*, vol. 43, no. 27, pp. 12 491–12 498, 2018. https://doi.org/10.1016/j.ijhydene.2018.04.194

[10] E. Baudoin, X. S. Bai, B. Yan, C. Liu, R. Yu, A. Lantz, S. M. Hosseini, B. Li, A. Elbaz, M. Sami, and et al., "Effect of partial premixing on stabilization and local extinction of turbulent methane/air flames," *Flow Turbul. Combust.*, vol. 90, no. 2, pp. 269–284, 2013. https://doi.org/10.1007/s10494-012-9414-z

[11] M. Faghih and Z. Chen, "The constant-volume propagating spherical flame method for laminar flame speed measurement," *Sci. Bull.*, vol. 61, no. 16, pp. 1296–1310, 2016. https://doi.org/10.1007/s11434-016-1143-6

[12] S. Liu, C. Zou, Y. Song, S. Cheng, and Q. Lin, "Experimental and numerical study of laminar flame speeds of CH4/NH3 mixtures under oxy-fuel combustion," *Energy*, vol. 175, no. 4, pp. 250–258, 2019. https://doi.org/10.1016/j.energy.2019.03.040

[13] A. Movaghar, R. Lawson, and F. N. Egolfopoulos, "Confined spherically expanding flame method for measuring laminar flame speeds: Revisiting the assumptions and application to C1-C4 hydrocarbon flames," *Combust. Flame*, vol. 212, no. 4, pp. 79–92, 2020. https://doi.org/10.1016/j.combustflame.2019.10.023

[14] X. Hu and H. Wei, "Experimental investigation of laminar flame speeds of propane in O2/CO2 atmosphere and kinetic simulation," *Fuel*, vol. 268, no. 1, p. 117347, 2020. https://doi.org/10.1016/j.fuel.2020.117347

[15] J. F. Brune, "The methane-air explosion hazard within coal mine gobs," *SME Trans.*, vol. 334, pp. 376–390, 2013. https://arlweb.msha.gov/REGS/Comments/2015-03982/AB85-Comm-9-1.pdf

[16] Q. Wang, H. Ma, Z. Shen, and Z. Guo, "Numerical simulation of premixed methane-air flame propagating parameters in square tube with different solid obstacles," *Procedia Eng.*, vol. 62, pp. 397–403, 2013. https://doi.org/10.1016/j.proeng.2013.08.081

[17] M. Jaeger, M. Hriberšek, N. Samec, Y. Guo, X. Wang, and F. Kokalj, "The numerical analysis of flame stability in case of premixed hydrogen-air combustion," *Appl. Therm. Eng.*, vol. 273, p. 126535, 2025. https://doi.org/10.1016/j.applthermaleng.2025.126535

[18] R. F. Cisneros and F. J. Rojas, "Determination of 12 combustion products, flame temperature and laminar burning velocity of Saudi LPG using numerical methods coded in a MATLAB application," *Energies*, vol. 16, no. 12, p. 4688, 2023. https://doi.org/10.3390/en16124688

[19] H. M. Mjbel, "Experimental and numerical study of the effect of Iraqi Liquefied Petroleum Gas (ILPG) on flame propagation speed," Master's thesis, University of Babylon, 2021.

[20] H. K. Versteeg, *An Introduction to Computational Fluid Dynamics: The Finite Volume Method*. Longmans Group Ltd, 2007.

[21] D. C. Wilcox, *Turbulence Modeling for CFD*. California, USA: DCW Industries, 1998.

[22] A. Sayma, *Computational Fluid Dynamics*. Ventus Publishing, 2009.

[23] R. J. Kee, F. Rupley, and J. Miller, "CHEMKIN II: A FORTRAN chemical kinetics package for the analysis of gas-phase chemical kinetics," Sandia National Lab. (SNL-CA), Livermore, CA, United States, Tech. Rep. SAND89-8009B, 1989.

[24] R. J. Kee, J. F. Grear, M. Smooke, and J. Miller, "A FORTRAN program for modeling steady laminar one-dimensional premixed flames," Sandia National Lab. (SNL-CA), Livermore, CA, United States, Tech. Rep. SAND85-8240, 1993.

[25] M. Akram, S. Kumar, and P. Saxena, "Experimental and computational determination of laminar burning velocity of liquefied petroleum gas-air mixtures at elevated temperatures," *J. Eng. Gas Turbines Power*, vol. 135, no. 9, p. 091501, 2013. https://doi.org/10.1115/1.4024798

**Nomenclature**

| | |
|---|---|
| $A$ | area, $m^2$ |
| $A_P$ | the pre-exponential factor |
| $C_P$ | Molar heat capacity at constant pressure, J/(mol·K) |
| $D$ | diameter, mm |
| $E$ | number of moles of component, mol |
| $E_a$ | activation energy, Cal/mol |
| $h$ | enthalpy, J |
| $k_f$ | reaction rate coefficient |
| $K_f$ | forward reaction rate, kmol/($m^2$·s) |
| $k'$ | kinetic energy of turbulent fluctuation per unit mass |
| $L$ | length, mm |
| $m$ | reaction rank |
| $M$ | mole fraction |
| $N$ | reaction rank |
| $p$ | pressure, bar |
| $\dot{Q}$ | volume flow rate mixture, $m^3$/s |
| $Re$ | Reynolds number |
| $R_0$ | molar gas constant, J/(mol·K) |
| $R$ | specific gas constant, J/(kg·K) |
| $R_x$ | rate of reaction, kmol/($m^3$·s) |
| $S_L$ | Stretched laminar flame speed, cm/s |
| $S_n$ | stretched laminar burning velocity, cm/s |
| $t$ | time, s |
| $u$ | velocity component in x direction, m/s |
| $u^*$ | (air mass (kg))/(fuel mass (kg)) |
| $v$ | velocity component in y direction, m/s |
| $V$ | inlet velocity, m/s |
| $X$ | number of moles of oxygen, mol |
| $Y$ | mass fraction |

Greek symbols

| | |
|---|---|
| $\epsilon$ | viscous dissipation rate of turbulent kinetic energy, $m^2/s^3$ |
| $\mu$ | dynamic viscosity, kg/(m·s) |
| $\rho$ | density, kg/$m^3$ |
| $\tau$ | viscous stress, N/$m^2$ |
| $\Phi$ | dissipation function |

Abbreviations

ER Equivalence ratio
CCC Cylindrical combustion chamber